DRAFT
ASME International Mechanical Engineering Congress and Exposition
IMECE2007
November 11-15, 2007, Seattle, Washington

IMECE2007-41604

# NUMERICAL ANALYSIS OF A PLANAR WAVE PROPAGATION BASED MICRO PROPULSION SYSTEM

**Ahmet Fatih Tabak**[*,1] **Serhat Yeşilyurt**[*,2]
[*]Sabanci University, Istanbul, Turkey
[1]tabak@su.sabanciuniv.edu, [2]syesilyurt@sabanciuniv.edu

## ABSTRACT

Micro-propulsion mechanisms differ from macro scale counterparts owing to the domination of viscous forces in microflows. In essence, propulsion mechanisms such as cilia and flagella of single celled organisms can be deemed as nature's solution to a challenging problem, and taken as a basis for the design of an artificial micro-propulsion system. In this paper we present numerical analysis of the flow due to oscillatory planar waves propagating on micro strips. The time-dependent three-dimensional flow due to moving boundaries of the strip is governed by incompressible Navier-Stokes equations in a domain with moving boundaries, which is modeled by means of an arbitrary Lagrangian-Eulerian formulation. The fluid medium surrounding the actuator boundaries is bounded by a channel, and neutral boundary conditions are used in the upstream and downstream. Effects of actuation parameters such as amplitude, excitation frequency, wavelength of the planar waves are demonstrated with numerical simulations that are carried out by third party software, COMSOL. Functional-dependencies with respect to the actuation parameters are obtained for the average velocity of the strip and the efficiency of the mechanism.

## INTRODUCTION

Propulsion mechanisms of microswimmers can be imitated artificial artificial propulsion systems to operate in low Reynolds number environments. A series of theoretical work focus on natural microswimmers and their actuation principles [1-6]. It was shown that inside highly viscous fluids with low Reynolds number, a conventional time reversible swimming action can not yield desired propulsive effect due to 'scallop theorem' [1].

Microswimmers, which usually are single celled organisms like spermatozoa, employ planar or helical wave propagation via their flagellum and cilia called organelles [2,3]. Periodic traveling-wave deformations on the biopolymer tail of the microorganism are the result of the balance between the bending stresses of the structure and the total stress in the fluid [4]. Sir Taylor presented asymptotic solutions of the flow for a sinusoidal wave propagating on an infinite inextensible sheet immersed in a viscous fluid [5]. Later, Katz presented an asymptotic solution for the infinite sheet placed inside a channel [6]. Childress [7] expanded the study to extensible sheet propulsion. Our previous work verifies asymptotic results of Taylor [5] and Katz [6] by means of numerical solution of the two-dimensional time-dependent Stokes flow due to plane waves traveling on a finite-length thin membrane inside a channel [8]. Although time irreversible wave propulsion is the method utilized by natural microswimmers, efficiency of these swimmers is found to be very low due to high shear losses [9].

Recent, theoretical and experimental studies on the propulsion of autonomous swimming robots utilize the biological mechanisms [10,11,12]. The mechanism is replicated artificially by wave propagation on an artificial tail made from magnetic filaments attached to blood-cells and driven by alternating external magnetic fields [13].

Traveling wave propagation on an electrically driven Nafion based tail in centimeter scale proved to be viable as a propulsion system [14] at low frequencies. Similarly, three-dimensional numerical investigation of surface acoustic waves created by interdigital transducers on a thin membrane was carried out as an actuation method at large frequencies despite the small amplitude of the acoustic waves [15]. Further-

more it is plausible to suggest that the wave propagation effect can also be sustained by a series of piezoelectric material replaced in series and driven out-of-phase with the shear mode of piezo strips [16,17,18].

Vertical motion of the fully submerged elastic rod tail causes dynamic high and low pressure regions shifting positions resulting in net fluid flow between. As the deformation shifts position accordingly with the propagation of traveling waves, high and low pressure regions in the vicinity of the membrane demonstrate consequential shifts which result in two-dimensional thrust effect. This resultant shifts cause a combinational force interactions between swimmer body and surrounding fluid which led to translation on both $x$ and $y$ axes, including rotation around z axis.

We present numerical simulations of 3D time-dependent motion of a conceptual swimming micro-robot,inside a liquid filled channel due to the propagation of sine-wave deformations on the long conical tail attached to a capsule. The motion of the swimmer is governed by rigid-body equation of motion which incorporates the forces and moments from the motion of the fluid governed by incompressible Navier-Stokes equations subject to continuity in a time-varying domain that has moving boundaries due to the motion of the tail as well as the motion of the robot. Mesh displacement due to moving boundaries of the membrane is modeled using arbitrary Lagrangian-Eulerian formulation [20] incorporating the Winslow method [21]. Effects of the amplitude, frequency, wave length and homogeneity of traveling waves on the speed, hydraulic power and efficiency are demonstrated.

## NOMENCLATURE

| Symbol | Description |
|---|---|
| **Latin Letters** | |
| $A$ | Area |
| $B_o$ | Maximum wave amplitude |
| $H$ | Channel height |
| $\mathbf{I}$ | Identity matrix |
| $L$ | Channel length |
| $P$ | Liquid pressure |
| $Q$ | Flow rate |
| $\mathbf{U}$ | Fluid velocity vector |
| $W$ | Width |
| $dy$ | Mesh deformation in $\Omega$ |
| $f$ | Excitation frequency [Hz] |
| $k$ | Wave number |
| $\ell_f$ | Membrane length |
| $\mathbf{n}$ | Surface normal vector |
| $t$ | Spatial time |
| $\mathbf{u}$ | Mesh velocity vector |
| $u,v,w$ | velocity components |
| $x,y,z$ | Spatial coordinates |
| **Functions and Groups** | |
| $B$ | Amplitude expression |
| min | Minimum function |
| Re | Reynolds Number |
| **Greek Letters** | |
| $\Pi$ | Mechanical Power exerted on fluid |
| $\Sigma$ | Mono directional full stress tensor |
| $\Omega$ | Domain occupied by fluid inside |
| $\eta$ | Percentage mechanical efficiency |
| $\lambda$ | Wave length |
| $\mu$ | Dynamic viscosity of liquid |
| $\rho$ | Liquid density |
| $\omega$ | Angular frequency |
| **Subscripts and Superscripts** | |
| $A.av$ | Area-averaged |
| $av$ | Time-averaged |
| $ch$ | Channel parameter |
| $f$ | Membrane parameter |
| in,out | Inwards/outwards direction |
| $m$ | Mesh parameter |
| T | Transpose |
| 0 | Characteristic scale |

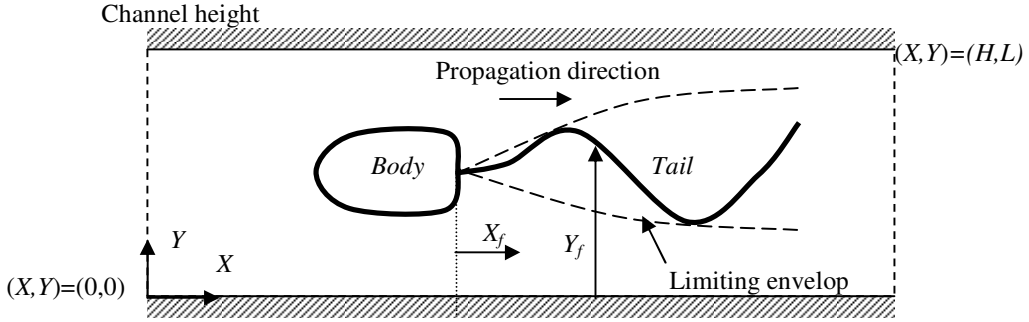


**Figure 1:** Plane-wave deformations traveling in the $x$-direction on the tail attached to the head of the robot; side-view in the $z$-direction on the $x$-$y$ symmetry plane. (butun denklemlerde x ve y kullaniliyor (cogunlukla) neden burada X ve Y kullaniyoruz. aciklamaktansa duzeltmek daha kolay...)

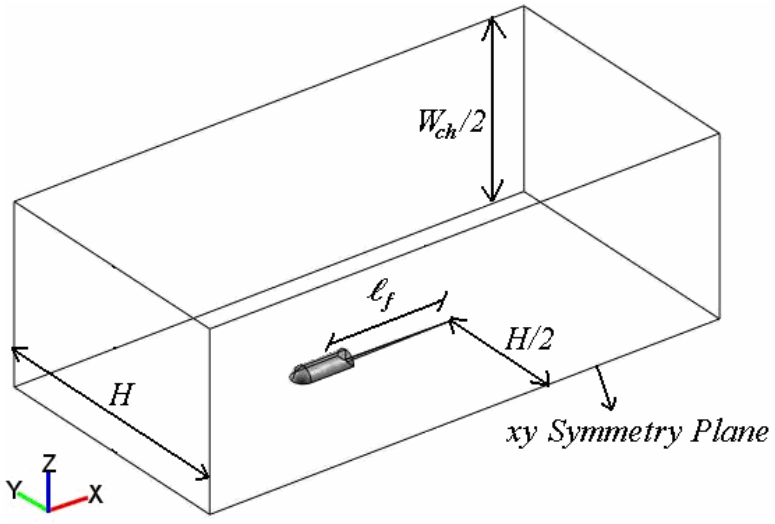


**Figure 3:** 3D view of conceptual swimming micro robot and the channel; cut into two symmetric pieces in the middle.

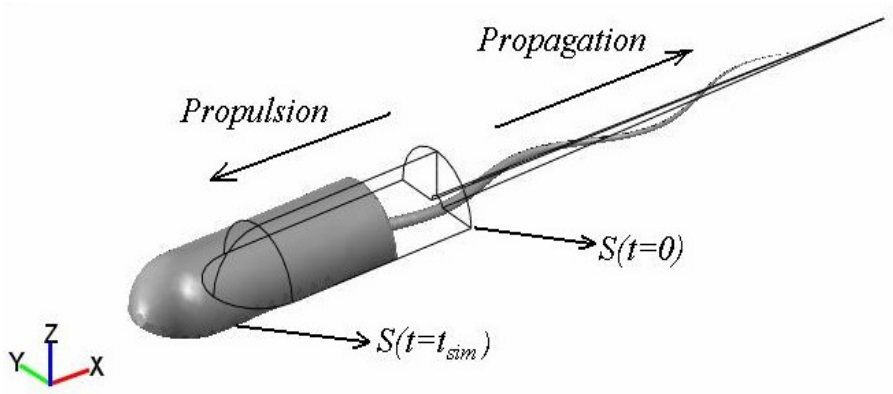


**Figure 4:** 3D view of conceptual swimming micro robot; net propulsion and wave propagation wakes place on opposite sides.

## METHODOLOGY

[buraya daha iyi bir giris paragrafi gerekiyor. 4 serbestlik derecemizin oldugu dogru degil!].

Motion of the tail, which is perpendicular to the wave propagation in the $x$-direction as shown in Fig. 1, is limited to the $y$-axis. and is given by a sinusoidal wave-form as a function of time, $t$, $x$-position on the tail, $x_f$, excitation frequency, $\omega=2\pi f$, wave number, $k=2\pi/\lambda$ and the amplitude $B$, i.e. we have

$$y_f\left(x_f,t\right)=B\sin\left(\omega t-kx_f\right),\quad x_f>0 \qquad (1)$$

In Eq. (1), $B=B(x,t)$ encompasses an envelope function for the extent of the deformations in the $y$-direction and keeps one end free while the other end is attached to the body at all times. Furthermore, to ensure zero initial conditions, an initial ramp of the amplitude of deformations is defined and restricted to the first full period:

$$B\left(x_f,t\right)=B_o\left(1-e^{-C_{sh}\left(x_f-x_{com}\right)}\right)\min\left(t,\frac{1}{f}\right) \qquad (2)$$

where $C_{sh}$ is the shape constant for amplitude envelope, $x_{com}$ is the $x$-coordinate of the center of mass which is on the rigid joint between tail and body.

Translation in $x$-direction is due to the thrust force exerted by the y-direction motion of the tail, and calculated from the equation of motion:

$$\ddot{x}_S=\frac{1}{M}\int_{S(t)}\Sigma_x dS \qquad (3)$$

where, $M$ is the mass of the neutrally buoyant swimmer and $\Sigma_x$ is the x-component of the full stress tensor, which is given by [23]:

$$\Sigma_x = \begin{bmatrix} \left(2\mu\dfrac{\partial u}{\partial X} - P\right) \\ \mu\left(\dfrac{\partial u}{\partial Y} + \dfrac{\partial v}{\partial X}\right) \\ \mu\left(\dfrac{\partial u}{\partial Z} + \dfrac{\partial w}{\partial X}\right) \end{bmatrix} \cdot \mathbf{n} \tag{4}$$

Translation in $y$-direction is calculated in the same manner as in Eq. (3) but with the $y$-component of the full stress tensor as follows

$$\ddot{y}_S = \frac{1}{M}\int_{S(t)} \Sigma_y dS \tag{5}$$

where

$$\Sigma_y = \begin{bmatrix} \mu\left(\dfrac{\partial u}{\partial Y} + \dfrac{\partial v}{\partial X}\right) \\ \left(2\mu\dfrac{\partial v}{\partial Y} - P\right) \\ \mu\left(\dfrac{\partial v}{\partial Z} + \dfrac{\partial w}{\partial Y}\right) \end{bmatrix} \cdot \mathbf{n} \tag{6}$$

Rotation around the center of mass, which is at the rigid connection between the body and the tail of the swimmer, in the $z$-direction is obtained from

$$\ddot{\theta} = \frac{1}{J}\int_{S(t)} M_z dS \tag{7}$$

where, $J$ is the moment of inertia, and the z-moment, $M_z$ is given by

$$M_z = \int_{S(t)} \left(\Sigma_x \sin\alpha + \Sigma_y \cos\alpha\right) r_{com} dS \,. \tag{8}$$

In Eq. (8) $r_{com}$ is the distance of a point on the swimer's surface from the center of mass of the swimmer, and α is the angle between the position vector of a point on the swimmer surface and the x-axis.

In order to model the flow around the swimmer-incompressible Navier-Stokes equations are used in the time-dependent domain $\Omega(t)$:

$$\rho\left(\frac{\partial \mathbf{U}}{\partial t} + (\mathbf{U} - \mathbf{u}_m)\cdot\nabla\mathbf{U}\right) = -\nabla P + \mu\nabla^2\mathbf{U} \tag{11}$$

$$\nabla\cdot\mathbf{U} = 0 \tag{12}$$

where $\mathbf{U}=[u,v,w]^T$ is the velocity vector, $P$ is pressure, ρ is density, and μ is the viscosity of the fluid. The time-dependent domain, Ω(t) deforms according to the moving boundaries of the swimmer. The $\mathbf{u}_m$ in Eq. (11) is the deformation velocity of the mesh used in the finite-element solution of Navier-Stokes equations. Since the mesh deforms only on the swimmer boundaries and remains fixed at the channel walls, inlet and outlet, a gradual deformation of the mesh is specified between the moving swimmer and the fixed boundaries.

Channel walls are subjected to no-slip boundary conditions at all times,

$$\begin{bmatrix} u(x,0,z,t) \\ v(x,0,z,t) \\ w(x,0,z,t) \end{bmatrix} = \begin{bmatrix} u(x,H,z,t) \\ v(x,H,z,t) \\ w(x,H,z,t) \end{bmatrix} = \begin{bmatrix} 0 \\ 0 \\ 0 \end{bmatrix}$$
$$\begin{bmatrix} u(x,y,0,t) \\ v(x,y,0,t) \\ w(x,y,0,t) \end{bmatrix} = \begin{bmatrix} u(x,y,W_{ch},t) \\ v(x,y,W_{ch},t) \\ w(x,y,W_{ch},t) \end{bmatrix} = \begin{bmatrix} 0 \\ 0 \\ 0 \end{bmatrix} \tag{13}$$

where $H$ is the channel height and $W_{ch}$ is the channel width. Tail does not move in $z$-direction as explained.

$$w(x_f, y_f, z_f, t) = 0 \tag{14}$$

In Eq. (14), $x_f$, $y_f$ and $z_f$ constitute the time-dependent position vector on the membrane; $y_f$ is given by Eq. (1). $Y$-velocity on the membrane is given by the time derivative of the displacement in Eq. (1):

$$v_f(x_f,t) = \frac{\partial y_f(x_f,t)}{\partial t} \tag{15}$$

Hence the velocity of a point on the surface of the swimmer is obtained by combining the time derivatives of Eq. (1), (3), (5) and (7).

$$\mathbf{U}_S = \begin{bmatrix} \dfrac{\partial x_S}{\partial t} + r_{com}\dfrac{\partial \theta_x}{\partial t} \\ \dfrac{\partial y_f}{\partial t} + \dfrac{\partial y_S}{\partial t} + r_{com}\dfrac{\partial \theta_y}{\partial t} \\ 0 \end{bmatrix}_{S(t)} \tag{16}$$

Inlet and outlet surfaces are specified as neutral [24] in all simulations which means

$$\left[-P\mathbf{I} + \boldsymbol{\sigma}\right]\cdot\mathbf{n}\Big|_{x=0,y,z,t} = 0 \tag{17}$$

$$\left[-P\mathbf{I} + \boldsymbol{\sigma}\right]\cdot\mathbf{n}\Big|_{x=L,y,z,t} = 0 \tag{18}$$

and $xy$-symmetry plane is designated as slip/symmetry [24] which means cancelling the tangential forces and the normal velocity on the designated boundary as in Eq. (19) and (20).

$$\left[-P\mathbf{I}+\boldsymbol{\sigma}\right]\cdot\mathbf{t}\Big|_{x,y,z,W_{ch}/2,t}=0 \tag{19}$$

$$\mathbf{U}\cdot\mathbf{n}=0 \tag{20}$$

where $\mathbf{t}$ is the tangential vector of the designated boundary.

For the flow at rest, all velocity components are specified as zero to guarantee complete stationary initial conditions.

$$u(x,y,z,0)=v(x,y,z,0)=w(x,y,z,0)=0 \tag{21}$$

Displacement of the deforming mesh is calculated from the prescribed displacement given by Eq. (1), (3), (5) and (7) by a rubber mesh function, which limits the deformation to exterior surfaces are constant at all times.

$$\Delta\mathbf{x}_m=\begin{bmatrix} x_S+r_{com}\theta_x \\ y_f+y_S+r_{com}\theta_y \\ 0 \end{bmatrix}\beta \tag{22}$$

where β is the rubber mesh function to limit the deformation within the channel [19]. The mesh displacement velocity, $\mathbf{u}_m$, in Navier-Stokes equation is found directly from the prescribed mesh deformation:

$$\mathbf{u}_m=\frac{\partial\Delta\mathbf{x}_\mathbf{m}}{\partial t} \tag{23}$$

Once $\mathbf{u}_m$ is obtained from Eq. (23), finite-element representation of Navier-Stokes and continuity equations, are solved subject to boundary conditions given by (),(),()... by the commercial finite element analysis package COMSOL, incorporating Intel's MKL that invokes the parallel, PARDISO solver in COMSOL.

Time averaged velocity components of the swimming microrobot are also found by integrating Eq. (16) and averaging it over simulation time. Tangential and rotational components of the velocity vector vanishes in time averaging and can be neglected. Swimmer's average velocity in the *x*-direction is given by,.

$$u_{S-av}=\frac{f}{2}\int_{t_o}^{t_o+2/f}\frac{dx_S}{dt}dt \tag{24}$$

Instantaneous rate of work done on the fluid by the deforming tail is the area integration of the product of the total *y*-stress and the local *y*-velocity, i.e.

$$\Pi(t)=\int_{A_f}\Sigma_y v_f\,dA_f \tag{25}$$

where $A_f$ is the tail's surface area. Similarly to Eq. (24), time-averaged rate of work done by the tail is calculated from:

$$\Pi_{av}=\frac{f}{2}\int_{t_o}^{t_o+2/f}\Pi(t)\,dt \tag{26}$$

Efficiency of the swimmer is calculated from the ratio between power need to overcome the *x*-force exerted on the overall swimmer and the power input calculated by Eq. (26) and (27) as described by Froude efficiency formulation [22]

$$F_{x-av}=\frac{f}{2}\int_{t_o}^{t_o+2/f}\int_{S(t)}\Sigma_x\,dS\,dt \tag{26}$$

$$\eta=\frac{F_{x-av}u_{S-av}}{\Pi_{av}} \tag{27}$$

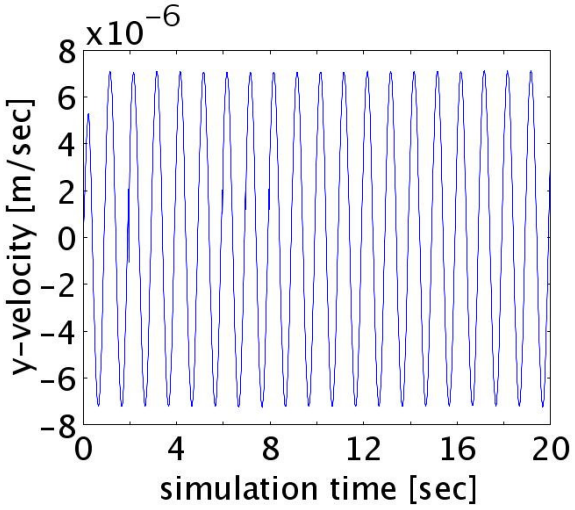


**Figure 5:** Instantaneous y-velocity of the swimmer.

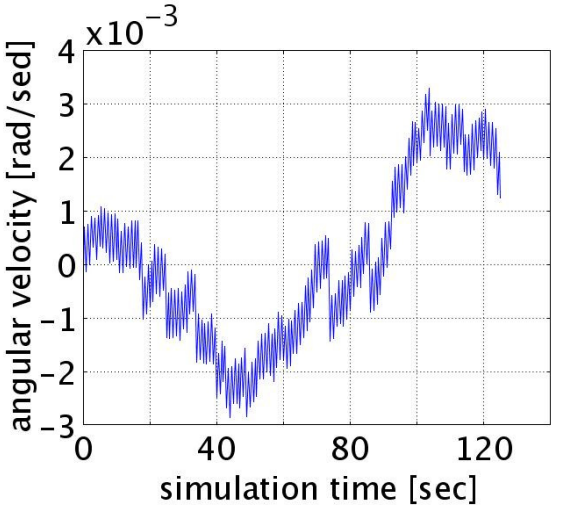

**Figure 6:** Instantaneous angular velocity of the swimmer.

## RESULTS

Reference dimensions and properties of the swimmer are provided in Table 1 for numerical results that are presented here. For each simulation, about 33000 linear equations are solved for at least 3 time units that correspond to 3 full cycles and at least 300 time steps after simulation outputs converge to the steady-periodic state within the first cycle. Each simulation takes between 2 to 3 hours on a double dual-core 3.7 GHz 64-bit Xeon workstation with 16GB of RAM running on SUSE Linux 10.0 operating system. Time-averaged quantities are obtained from integration over the last two cycles. Unless otherwise noted the base case used in the simulations corresponds to $\lambda = \ell_f / 2$, $B_o = 0.073x\lambda$, $f = 1$ Hz, and $C_{sh} = 6$.

| Name, symbol | Values/dimensions |
|---|---|
| $W_{ch}$ | $4x10^{-3}$ [m] |
| Channel Height, $H$ | $3x10^{-3}$ [m] |
| Channel Length, $L$ | $6x10^{-3}$ [m] |
| Tail Length, $\ell_f$ | $1.25x10^{-3}$ [m] |
| Head Length, $L_h$ | $6.25x10^{-4}$ [m] |
| Head Radius, $r_h$ | $1.25x10^{-4}$ [m] |
| Tail (membrane) width, $W_f$ | $2x10^{-5}$ [m] |
| Swimmer Mass Moment of Inertia, $J$ | $7.073456x10^{-12}$ [kg.m$^2$] |
| Mass of the Swimmer, $M$ | $1.713071x10^{-8}$ [kg] |
| Dynamic Viscosity of water, $\mu$ | $1.12x10^{-3}$ [Pa.s] |
| Density of water, $\rho$ | 999 [kg/m$^3$] |

**Table 1:** Simulation Constants

Figue 7 illustrates the flow field on the symmetry plane where large vortex formations take place. Figure 7 and 8 reveal that the swimmer pushes the fluid in the propulsion direction. The 'vortices' forming behind the tail is due to motion of the tip of the tail.

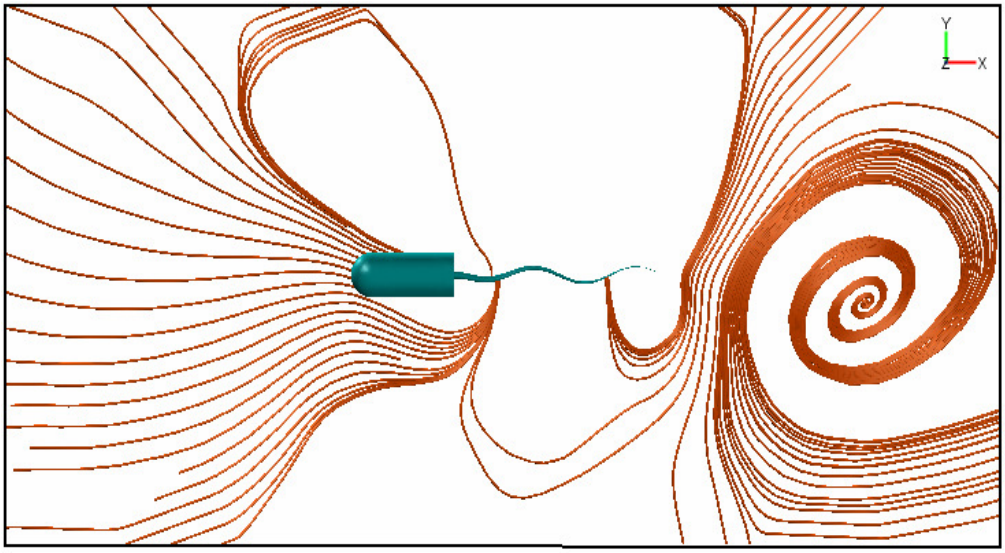


**Figure 7:** Swimmer micro robot with planar waves propagating on its tail and leaving a vortex trail.

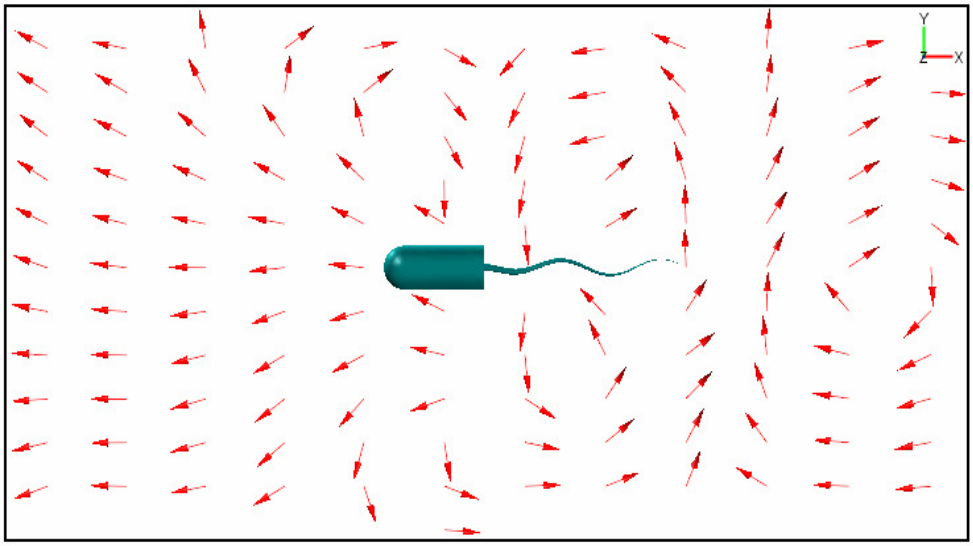


**Figure 8:** Normalized arrow plot demonstrating the flow field on the symmetry plane.

Figure 9 demonstrates the relationship between the amplitude and the average x-velocity of the micro swimmer for all the variables fixed at the base case except the amplitude. As amplitude increases the x-velocity increases quadratically with the amplitude. Figure 10 illustrates the effect of amplitude on power consumption which clearly shows that power consumption changes proportionally with the square of the change in amplitude. These results are in agreement with the asymptotical predictions stated by Taylor and Katz [5,6]. Figure 11, shows how swimmer efficiency behaves with respect to amplitude. It can be observed that efficiency increases very rapidly for small amplitudes but starts to plateau before reaching to 1%.

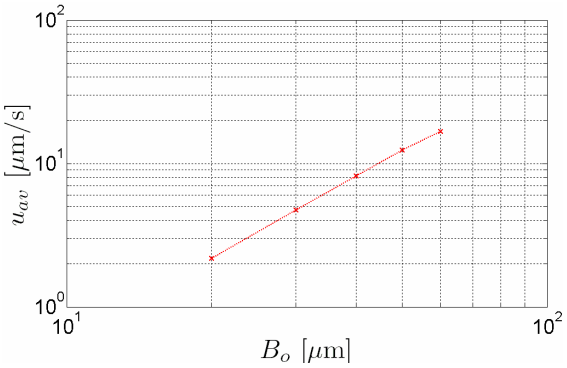


**Figure 9:** Wave amplitude vs. x-velocity for for λ = 625 µm, $f$ = 1 Hz and $C_{sh}$ = 6.

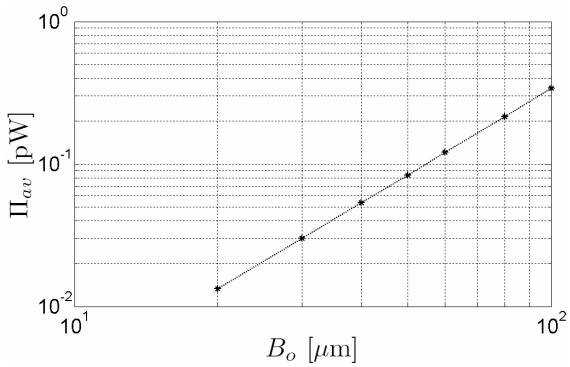


**Figure 10:** Wave amplitude vs. hydraulic power velocity for for λ = 625 µm, $f$ = 1 Hz and $C_{sh}$ = 6.

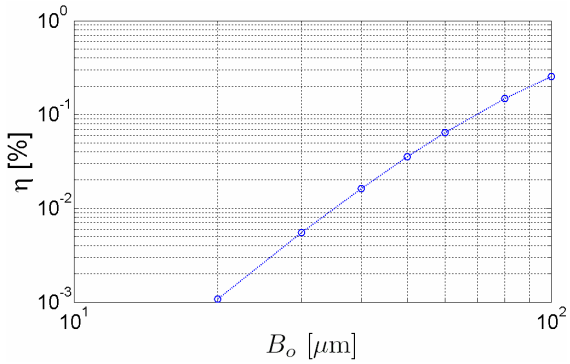


**Figure 11:** Wave amplitude vs. swimmer efficiency velocity for for λ = 625 µm, $f$ = 1 Hz and $C_{sh}$ = 6.

Figure 12 demonstrates the relationship between the frequency and the average x-velocity of the micro swimmer for all the variables fixed at the base case

except the frequency. As frequency increases the average x-velocity increases linearly with the frequency. Figure 13 illustrates the effect of the frequency on the power, and clearly shows that power increases proportionally with the square of the frequency. These results agree well with the asymptotical predictions stated by Taylor and Katz [5,6]. Figure 14, shows that the frequency does not affect the hydraulic efficiency of the swimmer.

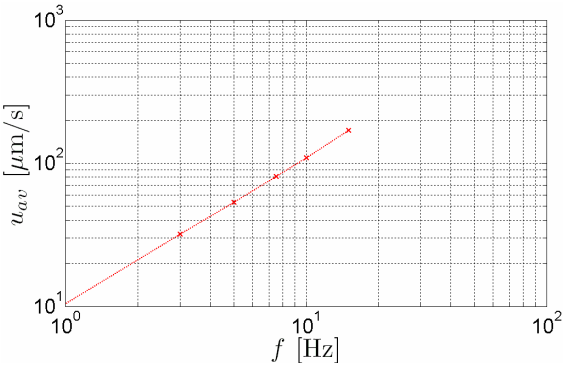


**Figure 12:** Driving frequency vs. Propulsion Velocity for λ = 625 μm, $B_o$ = 45.625 μm and $C_{sh}$ = 6.

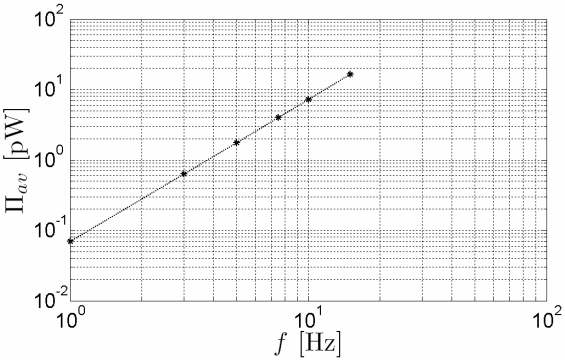


**Figure 13:** Driving frequency vs. Power Consumption for λ = 625 μm, $B_o$ = 45.625 μm and $C_{sh}$ = 6.

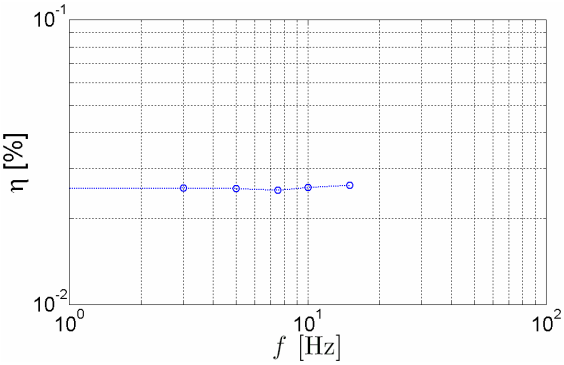


**Figure 14:** Driving frequency vs. Swimmer Efficiency for λ = 625 μm, $B_o$ = 45.625 μm and $C_{sh}$ = 6.

Figure 15 demonstrates the relationship between the wave length and the average x-velocity of the micro swimmer for all variables fixed at the base case except the wave length. As wave length increases average x-velocity increases linearly with the wave length agreeing well with the asymptotic calculations of Katz [6]. Figure 16 illustrates the effect of wave length on the power showing that as wave length increases the power increases with 3/2nd power of the wavelength. Figure 17, shows the effect of the wavelength on the swimmer's hydraulic efficiency, which is not as significant as the effect of the amplitude, but more important than the effect of the frequency. In our previous results for the 2D and 3D modeling of micropumps that utilize the

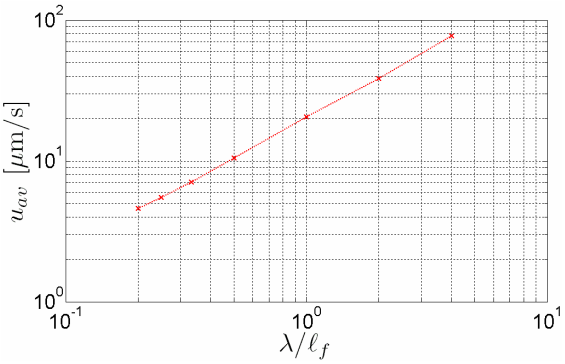


**Figure 15:** Ratio of Wave Length to Tail Length vs. Swimmer Velocity for $B_o$ = 45.625 μm, $f$ = 1 Hz and $C_{sh}$ = 6.

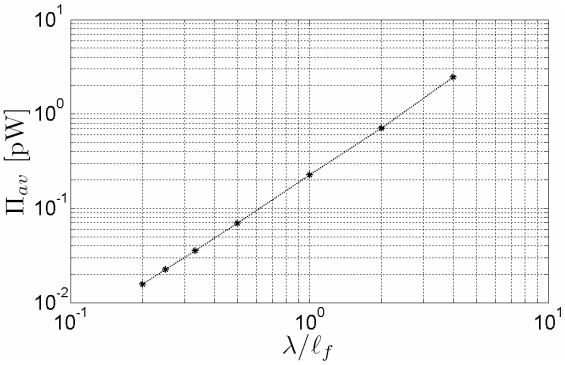


**Figure 16:** Ratio of Wave Length to Tail Length vs. Power Consumption for $B_o$ = 45.625 μm, $f$ = 1 Hz and $C_{sh}$ = 6.

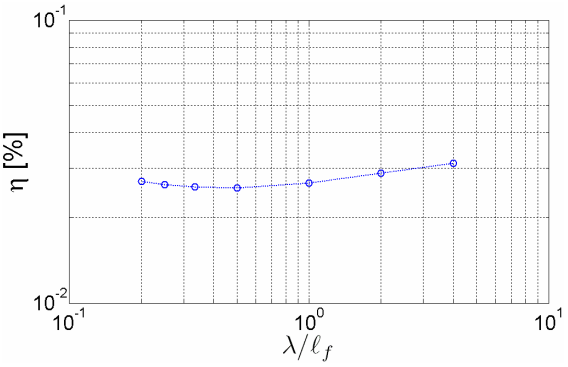


**Figure 17:** Ratio of Wave Length to Tail Length vs. Swimmer Efficiency for $B_o$ = 45.625 μm, $f$ = 1 Hz and $C_{sh}$ = 6.

Figure 18 display the relationship between the shape constant $C_{sh}$ and the average x-velocity of the micro swimmer for all variables fixed at the base case except the shape constant itself. The shape constant determines where the waves reach to their maximum amplitude away from the body of the swimmer. As $C_{sh}$ gets closer to 10 the wave propagation becomes more homogeneous on the tail hence the leveling behavior is expected. Similarly, in Figure 19 the same behavior for power consumption is observed. Consistent with the effect of the amplitude, as the constant increases efficiency increases approaching to a limit eventually.

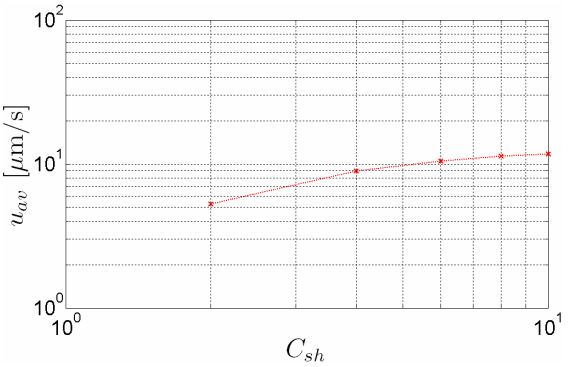


**Figure 18:** Shape Constant vs. Swimmer Velocity for λ = 625 μm, $B_o$ = 45.625 μm, $f$ = 1 Hz.

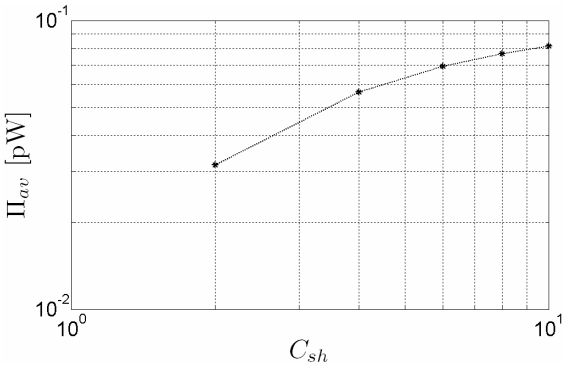


**Figure 19:** Shape Constant vs. Power Consumption for λ = 625 μm, $B_o$ = 45.625 μm, $f$ = 1 Hz.

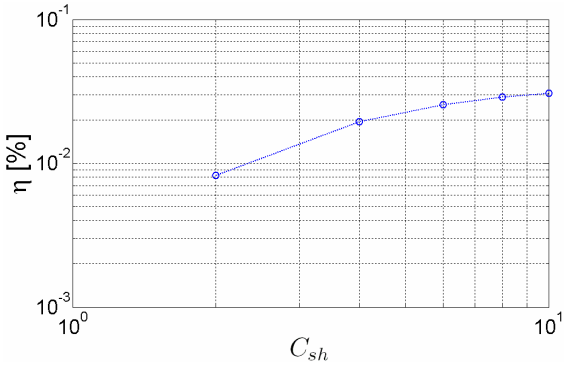


**Figure 20:** Shape Constant vs. Swimmer Efficincy for λ = 625 μm, $B_o$ = 45.625 μm, $f$ = 1 Hz.

## CONCLUSION

## ACKNOWLEDGMENTS

We kindly acknowledge the partial support for this work from the Sabanci University Internal Grant Program (contract number IACF06-00418).

## REFERENCES

[1] Purcell, E.M., 1977, "Life at Low Reynolds Number," American Journal of Physics, 45(1), pp. 3-11.

[2] Brennen, C., Winet, H., 1977, "Fluid Mechanics of Propulsion by Cilia and Flagella," Ann. Rev. Fluid Mech., 9, pp. 339-98.

[3] Gray, J., Hancock, G.J., 1955, "Propulsion of Sea-Urchin Spermatozoa," J. Exp. Biol., 32, pp. 802-814.

[4] Lowe, C.P., 2003, "Dynamics of Filaments: Modeling the Dynamics of Driven Microfilaments," Phil. Trans. R. Soc. Lond., B(358), pp. 1543-1550.

[5] Sir Taylor, G., 1951, "Analysis of the Swimming of Microscopic Organisms," Proc. Roy. Soc., A(209), pp. 447-61.

[6] Katz, D.F., 1974, "On the Propulsion of Micro-organisms Near Solid Boundaries," J. Fluid Mech., 64(1), pp. 33-49.

[7] Childress, S., 1981, Mechanics of Swimming and Flying, Cambridge Studies in Mathematical Biology, Cambridge University Press, New York, Chap. 3.

[8] Tabak, A.F., Yesilyurt, S., 2007, "Numerical Analysis of the 3D Flow Induced by Propagation of Plane-Wave Deformations on Thin Membranes inside Microchannels," Proceedings of the Fifth International Conference on Nanochannels, Microchannels and Minichannels, Puebla, Mexico.

[9] Sir Lighthill, J., 1975, Mathematical Biofluiddynamics, Society for Industrial and Applied Mathematics, USA, Chap. 3&4.

[10] Edd, J., Payen, S., Rubinsky, B., Stoller, M.L., Sitti, M., 2003, "Biomimetic Propulsion for a Swimming Surgical Micro-Robot," IEEE/RSJ Intelligent Robotics and Systems Conference, Las Vegas, USA.]

[11] Becker, L.E., Koehler, S.A., Stone, H.A., 2003, "On Self-Propulsion of Micro-Machines at Low Reynolds Number: Purcell's Three Link Swimmer," J. Fluid Mech., 490, pp.15-35.

[12] Wiggins, C.H., Goldstein, R.E., 1998, "Flexive and Propulsive Dynamics of Elastica at Low Reynolds Number," 80(17), pp. 3879-3882.

[13] Dreyfus, R., Baudry, J., Roper, M.L., Fermigier, M., Stoner, H.A., Bibette, J., 2005, "Microscopic Artificial Swimmers," Nature, 437, pp. 862-865.

[14] Kim, B., Kim, D.-H., Jung, J., Park, J.-O., 2005, "A Biomimetic Undulatory Tadpole Robot Using Ionic Polymer-Metal Composite Actuators," Smart Mater. Struct., 14, pp. 1579-1585.

[15] Nguyen, N.T., White, R.M., 1999, "Design and Optimization of an Ultrasonic Flexural Plate Wave Micropump Using Numerical Simulation," Sensors and Actuators, 77, pp. 229-236.

[16] Piefort, V., 2001, "Finite Element Modelling of Piezoelectric Active Structures. PhD Thesis submitted to Faculty of Applied Sciences," Université Libre De Bruxelles.

[17] Piefort, V., 2001, "Finite Element Modelling of Piezoelectric Active Structures. PhD Thesis submitted to Faculty of Applied Sciences," Université Libre De Bruxelles.

[18] Hofer, M., Lerch, R., 2002, "Finite Element Calculation of Wave Propagation and Excitation in Periodic Piezoelectric Systems," Mang, H.A., Rammerstorfer, F.G., Eds., Fifth World Congress on Computational Mechanics, Vienna, Austria.

[19] Tabak, A.F., 2007, "Micropropulsion System Design," MS Thesis to be submitted to Faculty of Engineering and Natural Sciences, Sabanci University, (in preparation).

[20] Duarte, F., Gormaz, R., Natesan, S., 2004, "Arbitrary Lagrangian-Eulerian Method for Navier-Stokes Equations with Moving Boundaries," Comput. Methods Appl. Mech. Engrg., 193, pp. 4819-4836.

[21] Winslow, A., 1967, "Numerical Solution of the Quisilinear Poisson Equations in a Nonuniform Triangle Mesh," J. Comp. Phys., 2, pp. 149-172.

[22] Sfakiotakis, M., Lane, D.M., Davies, J.B.C., 1999, "Review of Fish Swimming Modes for Aquatic Locomotion," IEEE Journal of Oceanic Engineering, 24(2), pp. 237-252.

[23] Landau, L.D., Lifshitz, E.M., 2005, Fluid Mechanics 2nd ed., Course of Theoretical Physics v.6, Elsevier Butterworth-Heinemann, Oxford, Chap. 2.

[24] COMSOL AB, 2005, Comsol Multiphysics Modelling Guide.

 